

Tracking Mobile Robot Trajectories Inside a Feedback Control Loop - Experimental Results

A. Steinicke

**DaimlerChrysler Research
FT3/AI
Alt-Moabit 96A
10559 Berlin**

J.Reuter

**IAV GmbH
AE-T11
Carnotstr.1
10587 Berlin**

S. Schönknecht

**TU-Berlin
Inst. f. Mech. Eng.
Str. d. 17 Juni
10623 Berlin**

Abstract

In this paper, we present a practical implementation of a real-time mobile robot pose tracker, using data from odometry and a gyroscope sensor. The data are fused to obtain a more reliable estimate, taking into account noisy and biased sensor readings from the wheel encoders and the gyroscope. The control error between the desired and the estimated position is used to stabilize the trajectory, driven by the robot. This is done by utilizing a flatness-based controller. The results obtained from experiments with a rebuilt mail-tractor demonstrate the good performance of both, the observer and the controller module. In this paper, we mainly focus on the pose tracking module.

1 Introduction

It is not the aim of this paper to present a new algorithm for solving the task of trajectory stabilization and concurrently estimating the position of the robot, but rather to show how results obtained in the position estimation community can be combined with a celebrated and from the theoretical point of view challenging control strategy, the flatness based control method. Many examples for how to use linear and nonlinear approaches for control of nonholonomic systems can be found in the literature [1][8][9][12][15][19][21][22], however, only a few strategies have found their way into real world robotics. A possible reason for this phenomenon may be the fact that currently in most robotics applications, the task of following a trajectory is reduced to the following of a given path, without making too restrictive constraints on the time- or velocity-profile, with which the path is driven. However, in recent years new path planning algorithms [2][10][13][14] start to take into account dynamic obstacles, other robots in multi-agent systems, as well as probabilities of obstacle occurrence and rendezvous problems. The feasibility of these algorithms depends on a precisely driven trajectory. Thus, steering a path seems not to be enough in the future, and therefore advanced control strategies are required. A possible field of operation are railway-stations or airports, where small autonomous tractor-trailer vehicles convey baggage and parcels. In our experiments a rebuilt tractor, which formally operated human-controlled on railway-stations carrying parcels, is used. The platform is described in the next section.

For position estimation, gyroscopes are widely used in the robotics area, and good results have been reported. The problems of this sensor are mainly related to scaling between angular speed and output voltage and thermal drift. In [3] several error-models were tested for thermal drift and bias estimation. Borenstein et al. investigated methods for error compensation and combined it with data from odometry, to improve dead-reckoning position estimation for a mobile robot [4][5][6][7]. In [17] redundancy of several inertial-sensors and gyroscopes were used to estimate parameters of errors like wheel-slippage and tyres deformation. Ojeda [16] uses a sophisticated calibration scheme to reduce thermal and scaling errors.

In this paper, we mainly focus on the pose tracking module. For completeness we present an experimental result obtained by combination of the observer and the controller. The reader is directed to [18] for more details. Most of the mobile robots in use are specially designed and carefully calibrated. However, our goal was to modify an already existing vehicle and convert it to an autonomous system. The platform has two driving wheels at the front and one wheel connected to the steering wheel at the rear. The driver's seat and the steering wheel were dismantled and a dc-motor with gear was fixed on the steering-column. The power of the driving dc-motor is 750W. Its shaft speed and the position of the shaft of the steering motor can be measured by two encoders. From these values odometry data are computed. The driving axis is equipped with a differential. Control of actors and sensors is performed by Infineon C176 /C166 microcontrollers. The weight of the platform is about 200kg. The main sources of error are gear backlash, high Coloumb friction of the tyres due to the heavy weight, as well as an inaccurate zero-position of the steering wheel.

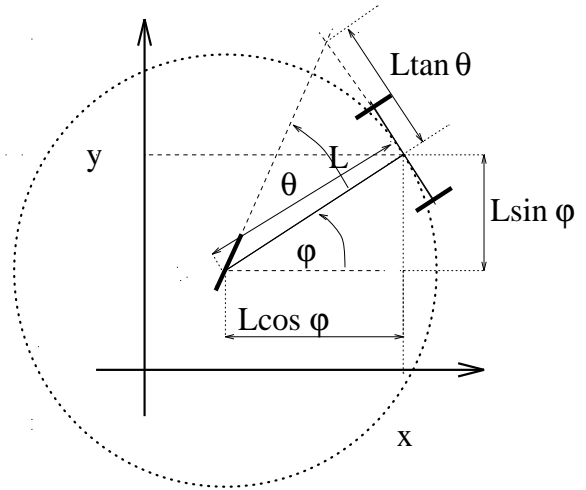


Fig. 1 Image of the experimental platform and associated kinematics

The nonholonomic kinematics are given by (ref. to fig. 1)

$$\begin{aligned} \dot{x}(t) &= v \cos \varphi \\ \dot{y}(t) &= v \sin \varphi \\ \dot{\varphi}(t) &= v \frac{\tan \theta}{L} \end{aligned} \quad (1)$$

Herein v is the velocity orthogonal to the front axis, θ is the steering angle and L is the length of the vehicle.

2 The gyroscope sensor

Although there is a huge number of algorithms for pose tracking (e.g. feature or grid-based) with different types of sensors described in the literature, most of all of these are too slow to be suitable to work as an observer in a feedback control loop structure. For a good and fast estimate of the vehicle's orientation, using data from a gyroscope is a proper choice. The output signal is proportional to the applied angular rate, thus, sudden disturbances, e.g. caused by lumpy patches on the ground and permanent errors due to wheel slippage and missaligned wheels are reflected in the output signal. However, for computing the orientation, the signal has to be integrated, causing an accumulation of errors. The advantages of the gyroscope are the continuous output signal, the high resolution and the large range of measurements. The offset, its drift and the influence of the temperature to the measurements are serious sources of inaccuracy, especially during long-time measurements. To fully exploit the used BASE¹-gyroscope, several reference measurements in

¹ British Aerospace System Equipment

preliminary experiments were taken. The data sheet, provided with the device, just specifies parameter boundaries, but gives few information about its individual characteristics.

2.1 Preliminary experiments

Thermal behaviour For solely investigating the thermal influence, the gyroscope was mounted tightly on the ground. No turning, meaning no input signal, was applied. Thus, the output should exactly be zero. During heating up the sensor, a change of the output was measured. One additional feature of the BASE-gyroscope is an extra output, which is to indicate temperature influences. This output was strongly affected by noise, and there was no clear dependency between the change of temperature and this signal, as long as the change of the temperature was small. Fig.2 and 3 show the results, during a heating and cooling between 20°C to 40°C.

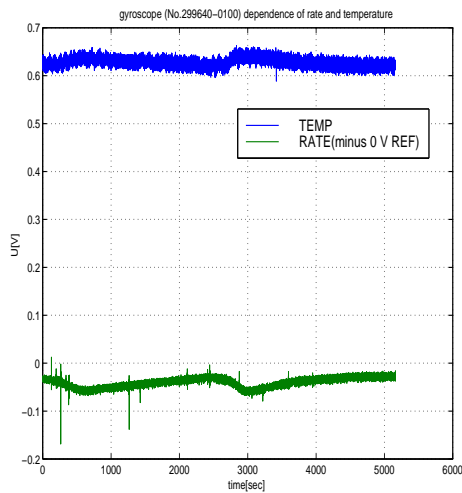


Fig. 2 Raw rate and temperature signals

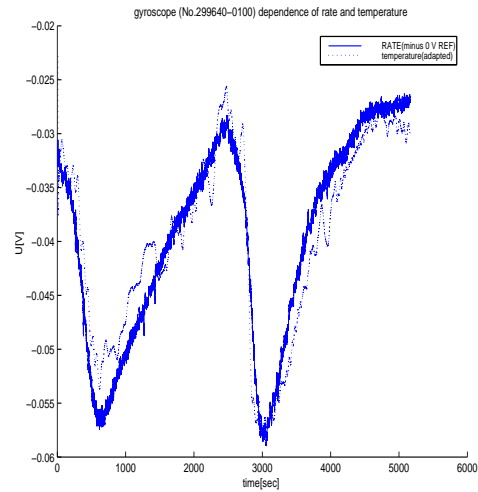


Fig. 3 Raw rate signal and filtered and adjusted temperature signal

The filtered temperature follows the disturbed rate signal when the warm air heated up the unit. However, this signal represents rather tendencies than reliable absolute values, especially during smaller changes of temperature and time periods of several 100 seconds. During operation of the robot, the variation of temperature is expected not to exceed 5°C, thus, this output signal could not be used. This is also proved by fig. 4, where the output values obtained with an identical measurement configuration, but in different experiments are plotted. It readily can be seen that in the upper plot the temperature output represents the drift quite well, while it differs in the lower plot. This clarifies the unpredictable correlation between these signals.

Long-term drift The used gyroscope belongs to the class of vibrating structure devices. A known phenomenon of these types of sensors is an offset voltage applied to the output signal. This offset causes the output to be different from zero, even if no movement is applied. Furthermore, the offset is drifting over time. This drift is not deterministic, and the gyroscope becomes more unreliable over time, ref. fig. 4. Although this drift depends on temperature, it even appears if there are no external temperature changes. This is one of the reasons why temperature influence cannot exactly be stated. The growing uncertainty is modelled by assuming an increasing standard derivation added to the rate signal. Where the offset over long terms (several hours) is unpredictable, it can be assumed to be constant, at least during short time intervals (several minutes). Thus, the rate output value is permanently measured during standstill. When the vehicle starts moving, the last measured value is stored. This value is subtracted from the rate output signal yielding the adapted gyroscope value.

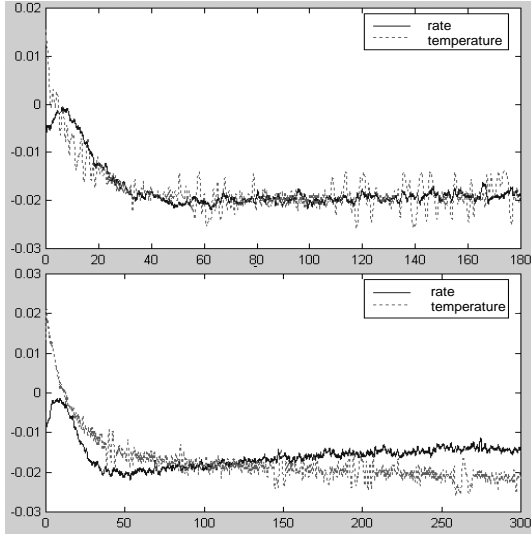


Fig. 4 Examples for variation of temperature and rate output signals.

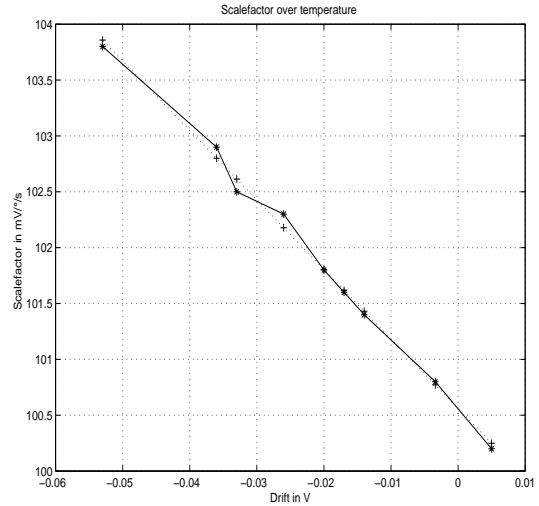


Fig. 5 Scale-factor affected by change of temperature

Scale factor The scale factor $F_s = \frac{U_{rate}}{\omega}$ gives the relation between the output voltage and the angular velocity around the sensitive axis as the sensor input. Ideally, the relationship between these quantities is exactly proportional meaning F_s is constant. In reality, it is a function of the temperature and even of the input signal itself. To find an appropriate scale function, a reference system was used. It consisted of a stepping motor with a resolution of 0.004° , which was controlled by a computer, to perform appropriate angular velocity profiles. The stepping motor drove a turnable platform, on which the gyroscope was mounted. The computer generated ramps with different rates, thus, the relation could be measured. For small angular rates ($< 7^\circ/s$) and constant temperature, the scale factor has a standard deviation less than 0.25%. Due to this result, a proportional dependence can be assumed. However, the scale factor is also influenced by the temperature. To investigate the impact of the temperature to the scale factor, not the temperature output signal, but the value of the offset was used. This value was determined by measuring the signal output just before the rotation started. Different offset values were reached due to heating up the device. The dependency can be seen from fig. 5.

The relation between the scale factor F_s and the current value of offset U_{ofs} was determined to

$$F_s = -62.22U_{ofs} + 100.56 \quad (2)$$

This relation is valid after a warm-up period of about 20 minutes.

3 The pose tracking module

3.1 Reference runs with odometry only

In this section, we describe experiments performed to investigate deterministic errors of the vehicle itself. Due to the error accumulation, the odometric position estimation based on the wheel encoders only, yields a big difference between the real position and the calculated one. The main reason for this is the displacement of the zero position of the steering wheel, resulting in a constant left drift of the vehicle. Additionally, the steered wheel has a small backlash. To measure the displacement, special trajectories were constructed. Curves with different radii but with 90° turning angle in common were driven with different velocities. 3 radii times 3 velocities yielded 9 curves for each direction ($\pm 90^\circ$ turning angle). In these experiments, only the final real position could be measured. In a first approach a linear dependence between the final position error and the velocity and the radius of the curves could be found. Although this dependency was not used further on, it enables us to get a deeper insight of this more complex relationship, [20]. The entire measurements were used to describe the displacement and the backlash in the following section.

3.2 Zero angle displacement

The zero angle displacement consists of an almost constant part d and a variable addendum a . The constant d renders the displacement of the steered wheel to its zero position. A drift to the left during a commanded straight line forward run has been observed. The variable a is constant in its absolute value, but changes sign according to the sign of the curvature. The values of these two variables were determined from the reference runs. In these runs, the final position φ_r after N steps is specified through the discrete kinematics with sample time T .

$$\varphi_r = \frac{T}{L} \sum_{k=1}^N v_i \tan \theta_i \quad (3)$$

The missalignment is modeled by adding an offset s to the steering angle θ in every time step. The true position φ_w after N steps yields

$$\varphi_w = z + \varphi_r = \frac{T}{L} \sum_{k=1}^N v_i \tan(\theta_i + s). \quad (4)$$

Thus, z renders the difference between the true and the calculated position. Developing eq. 4 in a Taylor series, assuming s to be sufficiently small, neglecting higher order terms and finally subtracting eq. 3, leads to

$$z = \varphi_w - \varphi_r = s \frac{T}{L} \sum_{k=1}^N \frac{v_i}{\cos^2 \theta_i}. \quad (5)$$

Now the value of s can be determined for every single run from eq. 5. Using the results from section 3.1, 9 values of s for every turning direction are obtained. Because of the backlash, s lies in two areas, which depends on the sign of the curvature. All measurements of one direction were averaged, yielding

$$\bar{s} = \bar{d} + \text{sign}(\theta)\bar{a}. \quad (6)$$

To take into account the variation of s , one of these two variables was taken into the model. Hence d is the third state with its own variance, see eq. 8.

3.3 Sensor data fusion

To calculate an estimate of the orientation angle, three measurements were used. The rate output of the gyroscope ω_G , the value of the steered wheel encoder θ and the velocity v . Different models, all of the form

$$x_{k+1} = f(x_k, u_k) \quad (7)$$

were investigated. Here we only present the best results, obtained by a model with state vector elements orientation angle φ , the angular velocity $\omega = \dot{\varphi}$ and the part d of the zero angle missalignment.

$$\begin{pmatrix} \varphi_{k+1} \\ \omega_{k+1} \\ d_{k+1} \end{pmatrix} = \begin{pmatrix} \varphi_k + T\omega_k \\ \frac{v_k \tan(\theta_k + d_k + \text{sign}(\theta_k)a_k)}{L} \\ d_k \end{pmatrix} \quad (8)$$

A Kalman-filter was used to calculate a new estimate, fusing the old one and the new measurements, as follows.

3.4 Kalman-filter

The measurement equation is given by

$$z_k = \omega_{Gyrk} = (0 \ 1 \ 0) \begin{pmatrix} \varphi_k \\ \omega_k \\ d_k \end{pmatrix} \quad (9)$$

The input for the Kalman filter are the three values ω_G , θ and v . Here ω_G is the adapted output signal from the gyroscope, see section 2.1. Because there are nonlinear terms in the model eq. 8, the extended Kalman-filter has to be used. The Jacobi Matrix of f is given by

$$J_k = \frac{f(x_k, u)}{dx} \Big|_{x=x_k} = \begin{pmatrix} 1 & T & 0 \\ 0 & 0 & c \\ 0 & 0 & 1 \end{pmatrix}, \quad (10)$$

where

$$c = \frac{v_k}{L \cos^2(\theta_k + d_k + \text{sign}(\theta_k) * a_k)}.$$

The initial values are chosen to

$$x_0 = \begin{pmatrix} 0 \\ 0 \\ -0.0197 \end{pmatrix} \quad (11)$$

where the third value, representing d , is obtained from the reference experiments and according computation in section 3.1 and 3.2. The choice of the required covariance matrices is made by a heuristic procedure to minimize the estimation errors for several experimental runs. The covariance matrix for the system noise is chosen to

$$Q = \begin{pmatrix} 0.07\text{cm}^2 & 0 & 0 \\ 0 & 0.07\text{cm}^2 & 0 \\ 0 & 0 & 1e-9\text{rad}^2 \end{pmatrix}, \quad (12)$$

while the variance of the measurement noise is selected to

$$R_0 = 0.0009\text{rad}^2/\text{s}^2. \quad (13)$$

To take into account the growing uncertainty of the gyroscope, the variance is increased in every time step by

$$\Delta R = 0.00047\text{rad}^2/\text{s}^2.$$

4 Experimental pose tracking results

With the implementation of these parameters, some further experiments were taken.

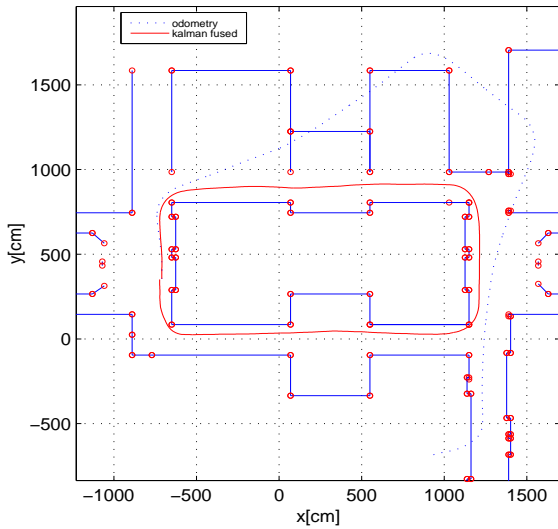


Fig. 6 Experiment 7 (see table 1), robot is running clockwise

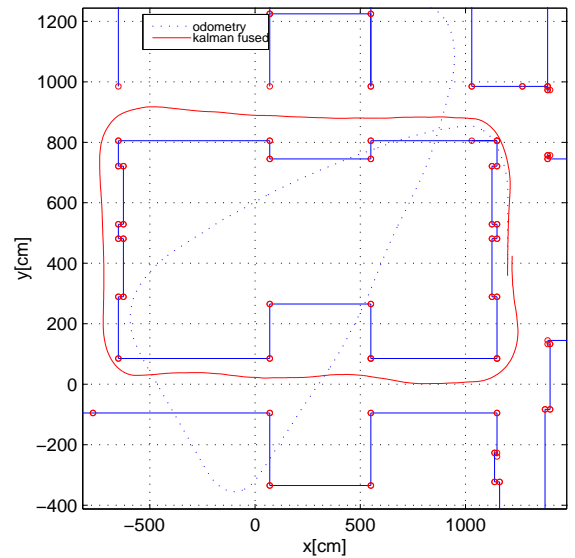


Fig. 7 Experiment 5 (see table 1), robot is running counterclockwise

In Fig. 6 the robot starts from coordinates $(-700, 350)$ moving clockwise. In Fig.7 the robot starts from coordinates $(1200, 350)$ running counterclockwise. The length of each path is about 65m.

The following table shows the finally estimated orientation of several runs together with the relative estimation error. The 2nd column contains the real values, determined by measurements on the ground. Columns 3 and 4 present the results obtained when using the Kalman-filter. The 5th and 6th column show the integrated signal of the gyroscope divided by the scale factor. The next two columns show the estimate when calibrated encoder data are used, i.e. the displacement is taken into account. Column 9 and 10 contain data obtained by using pure odometry, without regarding the displacement. The last column represents the absolute error of the fused estimate normalized subject to the length of the driven path.

Table 1. Orientation errors for the performed experiments

No.	Measuerd	Fused	rel. Err. [%]	gyroscope	rel. Err. [%]	encoder adjusted	rel. Err. [%]	odometry	rel. Err. [%]	Err _p [°/m]
1	91.4	91.6	0.2188	92.2	0.8753	92.3	0.9847	57.2	-37.4179	0.010
2	-90.0	-90.6	0.6667	-90.7	0.7778	-90.8	0.8889	-119.0	32.2222	-0.031
3	180.9	180.1	-0.4422	183.3	1.3267	178.5	-1.3267	184.0	1.7137	-0.059
4	-360.0	-363.3	0.9167	-364.2	1.1667	-362.1	0.5833	-439.3	22.0278	-0.056
5	-361.1	-360.4	-0.1939	-360.1	-0.2769	-360.7	-0.1108	-439.7	21.7668	0.012
6	-359.6	-359.1	-0.1390	-358.9	-0.1947	-358.3	-0.3615	-439.6	22.2469	-0.008
7	359.8	359.5	-0.0834	360.5	0.1946	357.5	-0.6392	261.0	-27.4597	-0.005
8	363.4	361.0	-0.6604	362.2	-0.3302	358.8	-1.2658	265.6	-26.9125	-0.042
9	359.7	359.5	-0.0556	361.5	0.5004	356.7	-0.8340	266.5	-25.9105	-0.003

5 Combining estimation and control

The position estimate using the Kalman-filter is obtained in real time. It is used to compute the control error between the desired and the actually estimated pose (position and orientation). Please refer to [18] for further details. In fig. 8 the desired and driven paths are plotted. In this experiment, for $t = 0$ we placed the robot in a certain distance from the reference path to obtain an initial error. The dots present the estimated position in every 4th time instance. Thus, it also provides information about the velocity profile. It can be seen that the velocity is increased until the desired trajectory is reached, and after this, it remains nearly constant. The initial control error decreases down to about 5cm, representing the tracking error of the controller. This error being constant means exactly following the trajectory with a short delay.

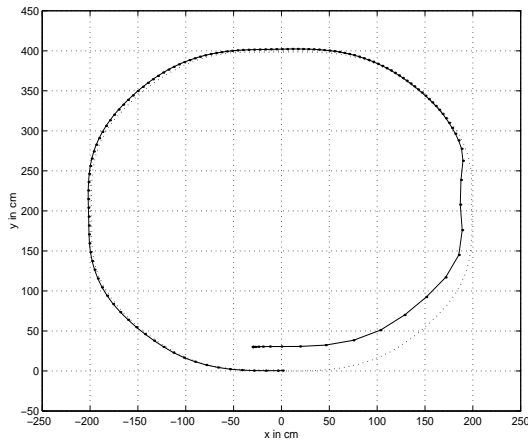


Fig. 8 Desired (dashed) and actually driven trajectory

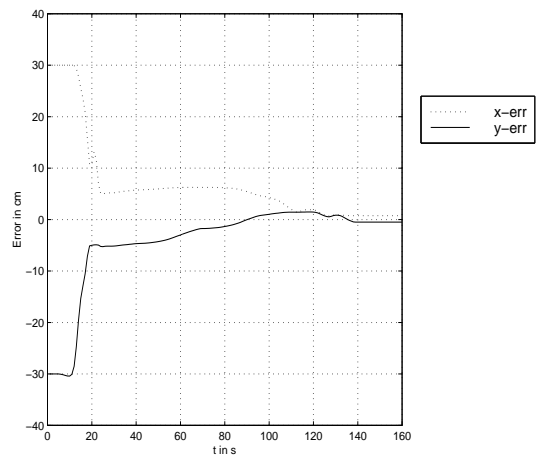


Fig. 9 Error in x- (dashed) and y- direction

6 Discussion and conclusions

The presented results show that pose tracking based on odometry can significantly be improved by using a fusion of encoder and gyroscope data. The algorithm is fast and easy to implement. Computation of the pose tracking and control modules were performed inside a 10ms task. To this end we did not utilize more sophisticated estimation procedures, e.g. the methods presented in [7] or [11]. The differences in the results achieved for the full turns (360°), mainly stem from different kinds of operating the joystick. The results get as better as more turning is commanded. This is due to the fact that during straight line motion the steering wheel moves inside the backlash. This is not reflected by the encoder signals. More accurate investigations would require measurements not only of the final position, but of the true position in every time step during the reference runs. However, in this paper we show that precise and expensive calibration systems can be avoided. The absolute accuracy and reliability of the IPEC-algorithm from [5] could not completely be reached. However, they use a platform consisting of two smaller, differential drive platforms which reference each other. Nevertheless, the factor of improvement of the orientation estimate reached here is not worse than the one from IPEC, amounting here up to 500 (run no. 9 in table 1).

In recent years fiber-optics gyros became available. Excellent results have been presented in [16]. It should be mentioned that the price of the sensor they used is more than four times higher, than the one we used here.

The combination of pose tracking and control enables the robot to precisely drive a given geometric path, together with the desired velocity profile. In case of initial errors or in case of loosing track, the controller forces the robot back to the planned trajectory. However, the controller uses the estimated position as a true input. Thus, it cannot be better than the pose tracker. From fig. 8 it can be seen that the controller works extremely well, as long as the observer accurately estimates the position. Future research can be directed by including more nonlinear models for offset and drift estimation.

References

1. A. Astolfi. Exponential Stabilization of a Mobile Robot. Automatic Control Laboratory ETH-Zürich.
2. G. Azarm, K. Schmidt. Integrated Mobile Robot Motion Planning and Execution in Changing Indoor Environments. In *International Conference on Intelligent Robots and Systems*, pages 306–313, 1994.
3. B. Barshan and H.F. Durrant-Whyte. Inertial Navigation Systems for Mobile Robots. *IEEE Transaction on Robotics and Automation*, 11(3):328–342, June 1995.
4. J. Borenstein. Experimental Evaluation of a Fiber Optics Gyroscope for Improving Dead-reckoning Accuracy in Mobile Robots. In *IEEE Proceedings of the International Conference on Robotics and Automation*, pages 963–969, 1998.
5. J. Borenstein. Experimental Results from Internal Odometry Error Correction with the OmniMate Mobile Robot. *IEEE Transaction on Robotics and Automation*, 14(6):963–969, December 1998.
6. J. Borenstein and L. Feng. Gyrodometry: A New Method for Combining Data From Gyros and Odometry in Mobile Robots. In *IEEE Proceedings of the International Conference on Robotics and Automation*, pages 423–428, 1996.
7. J. Borenstein and L. Feng. Measurement and Correction of Systematic Odometry Errors in Mobile Robots. *IEEE Transaction on Robotics and Automation*, 12(6):869–880, December 1996.
8. F. Bullo and R.M. Murray. Experimental Comparison of Trajectory Trackers for a Car with Trailers. Technical report, California Institute of Technology, 1995.
9. C. Canudas and Sjørdalen O.J. Exponential Stabilization of Mobile Robots with Nonholonomic Constraints. *IEEE Transaction on Automatic Control*, 37(11):1791–1796, 1992.
10. A. Chakravarthy and D. Ghose. Obstacle Avoidance in a Dynamic Environment: The Collision Cone Approach. *IEEE Transaction of Systems Science and Cybernetics*, 28(5):562–574, September 1998.
11. M.S. Grewal et al. Application of Kalman-Filtering to the Calibration and Alignment of Inertial Navigation Systems. *IEEE Transaction on Robotics and Automation*, 36(1):4–13, January 1991.
12. Y. Kanayama and F. Fahroo. A New Line Tracking Method for Nonholonomic Vehicles. In *IEEE International Conference on Robotics and Automation*, pages 2908–2913, 1997.
13. R. Kimmel, N. Kiryati, and A.M. Bruckstein. Multivalued Distance Map for Motion Planning on Surfaces with Moving Obstacles. *IEEE Transaction on Robotics and Automation*, 14(3):427–436, June 1998.
14. E. Kruse, R. Gutschke, and F.M. Wahl. Bahnplanung in dynamischen Umgebungen: Berechnung und Minimierung von Kollisionswahrscheinlichkeiten auf Basis statistischer Daten. Technical report, Institut für Robotik und Prozessinformatik, TU-Braunschweig, 1994. Bericht Nr. 446.

15. Y. Ma, J. Košecká, and S.S. Sastry. Vision guided navigation for a nonholonomic mobile robot. *IEEE Transaction on Robotics and Automation*, 15(3), 1999.
16. L. Ojeda et al. Precision-Calibration of Fiber-optics gyroscopes for Mobile Robots Navigation. In *IEEE International Conference on Robotics and Automation*, pages 2064–2067, 2000.
17. S. Scheding et al. An Experiment in Autonomous Navigation of an Underground Mining Vehicle. *IEEE Transaction on Robotics and Automation*, pages 85–95, 1999.
18. S. Schönknecht et al. Tracking and Stabilizing Mobile Robot Trajectories - Experimental Results. In *7. Int. Symposium on Models and Methods in Automation and Robotics*, 2001.
19. F. Sekhavat et al. Motion Planning and Control For Hilare Pulling A Trailer: Experimental Issues. In *IEEE International Conference on Robotics and Automation*, pages 3306–3311, 1997.
20. A. Steinicke. Multi-Sensor Integration zur Verbesserung der Orientierungsschätzung bei einem mobilen autonomen Roboter. Studienarbeit, TU Berlin, 2000.
21. G. Walsh, D. Tilbury, S. Sastry, R. Murray, and J.P. Laumond. Stabilization of Trajectories for Systems with Nonholonomic Constraints. 39(1), 1994.
22. J.M. Yang and J. H. Kim. Sliding Mode Control for Trajectory Tracking of Nonholonomic Wheeled Mobile Robots. *IEEE Transaction on Robotics and Automation*, 15(3), 1999.